

Magnetic fabric, welding texture and strain fabric in the Nuraxi Tuff, Sardinia, Italy

L. Pioli · R. Lanza · M. Ort · M. Rosi

Received: 26 February 2006 / Accepted: 9 December 2007 / Published online: 22 January 2008
© Springer-Verlag 2008

Abstract Anisotropy of magnetic susceptibility (AMS) has been used to interpret flow directions in ignimbrites, but no study has demonstrated that the AMS fabric corresponds to the flow fabric. In this paper, we show that the AMS and strain fabric coincide in a high-grade ignimbrite, the Nuraxi Tuff, a Miocene rhyolitic ignimbrite displaying a wide variability of rheomorphic features and a well-defined magnetic fabric. Natural remanent magnetization (NRM) data indicate that the magnetization of the tuff is homogeneous and was acquired at high temperatures by Ti-magnetite crystals. Comparison between the magnetic fabric and the deformation features along a representative section shows that AMS and anisotropy of isothermal remanent magnetization (AIRM) fabric are coaxial with and reproduce the shape of the strain ellipsoid. Magnetic tests and scanning electron microscopy observations indicate that the fabric is due to trails of micrometer-size, pseudo-single domain, magnetically interacting magnetite crystals. Microlites formed along discontinuities such as shard rims

and vesicle walls mimicking the petrofabric of the tuff. The fabric was thus acquired after deposition, before late rheomorphic processes, and accurately mimics homogeneous deformation features of the shards during welding processes and mass flow.

Keywords High-grade tuff · Magnetic anisotropy · Laminar flow · Rheomorphism · Welding · Sardinia

Introduction

The analysis of the magnetic fabric of rocks has been used for purposes such as geodynamic reconstructions, stratigraphic correlation and sedimentological studies. Moreover, anisotropy of magnetic susceptibility (AMS) can be used as a proxy for the textural analysis of rocks (Rochette et al. 1992; Borradaile and Henry 1997). The AMS fabric of a rock depends on the anisotropy of the grains it contains, on their spatial arrangements, and on the magnetic interaction between ferromagnetic grains (distribution anisotropy). Compared to traditional thin section studies, an individual AMS measurement is volumetrically more representative (it is performed on a specimen with volume of about 11 cm³), more sensitive, and less time consuming. On the other hand, since AMS is a complex function of several factors, such as mineralogy, grain shape, size, distribution and concentration, it cannot be used to describe sub-fabric variability of the rock without supporting information from other techniques, and its use for sedimentological and structural modeling purposes must be calibrated through field-based studies of facies and stratigraphy of the rock (Rochette et al. 1992).

This work explores the potential use of magnetic fabric as a strain indicator and addresses the origin of the

Editorial responsibility: R. Cioni

L. Pioli (✉) · M. Rosi
Dipartimento di Scienze della Terra, Università di Pisa,
Via S. Maria 53,
56126 Pisa, Italy
e-mail: pioli@dst.unipi.it

R. Lanza
Dipartimento di Scienze della Terra, Università di Torino,
Via Valperga Caluso 35,
10125 Torino, Italy

M. Ort
Environmental Sciences and Geology,
Northern Arizona University,
P.O. Box 4099, 86011 Flagstaff, AZ, USA

fabric and its relations with welding texture and rheomorphic facies in the Nuraxi Tuff, a well-exposed, widespread lava-like ignimbrite located in SW Sardinia (Italy) that displays conspicuous flow structures, variability of welding and crystallization facies and a well-defined magnetic fabric. More general implications of our results for the interpretation of magnetic fabric of welded ignimbrites are also discussed in the conclusion section.

Magnetic fabric of welded ignimbrites

Investigation of the magnetic fabric of welded ash-flow tuffs has shown it is mainly related to Ti-magnetite grains and may be controlled by a combination of depositional processes, paleo-flow directions and strain (Elwood 1982; Ort et al. 2003). The AMS ellipsoids of ash-flow tuffs are generally oblate with low anisotropy and wide scattering of data, perhaps due to magnetic ‘pollution’ by lithic clasts (Le Pennec et al. 1998), or to low anisotropy of the fabric. Improved clustering of k_3 axes (poles of the magnetic foliation plane) is expected for welded tuffs due to welding compaction. The fabric has been explained by hydrodynamic alignment of grains as in lava flows and dikes (Hrouda 1982; Knight and Walker 1986; Jackson and Tauxe 1991; Tarling and Hrouda 1993; Herrero-Bervera et al. 2001), or to nucleation of groundmass Fe-oxide microcrystals that formed either in the glass or at the vesicle walls at high temperatures (Schlinger et al. 1988; Wolff et al. 1989; Thomas et al. 1992; Palmer et al. 1996; Palmer and MacDonald 1999). However, a more comprehensive interpretation of the data is still problematic as it is not clear when and how the fabric formed, nor what its relation is with the petrofabric. This fact has substantially lowered the potential applications of magnetic fabric investigations of ignimbrites, which are mainly confined to determination of paleo-flow directions and location of source vents (Palmer and MacDonald 1999). More information and quantitative application to the description of the strain-and petrofabric are expected when AMS data are linked to supplementary magnetic evidence and detailed petrographic observation. In this study we rigorously test the origin of the magnetic fabric and show that AMS can be used with confidence as a proxy for flow fabric. We also discuss both macro and microscopic strain fabrics and magnetic properties and show that they are directly related to each other.

Among welded ignimbrites, lava-like, intensely rheomorphic tuffs are particularly suitable for these studies since they generally display high susceptibility and well-defined anisotropy, providing high-quality magnetic and structural dataset.

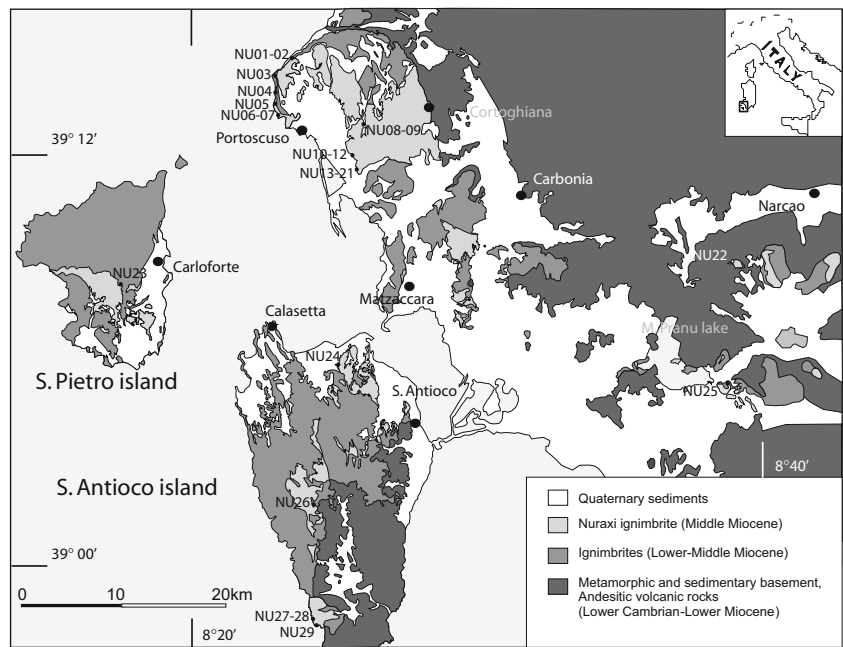
Microstructural studies of welded ignimbrites

The rheology of a welded ignimbrite at temperatures exceeding the glass transition is similar to that of a lava flow. When the compaction of the tuff is complete the original clastic nature of the material no longer affects the rheology of the liquid since the primary particles cannot flow and deform independently from one another and inhomogeneities in the flow are related to crystal and lithic grains. Strain studies on welded ignimbrites by Sheridan and Ragan (1976) demonstrated that, after all pore space is eliminated (compactional welding is complete), equal volume deformation of the deposit is related to shear flow due to topographic irregularities in the substrate. Since the compactional strain has uniaxial symmetry, the strain ellipsoid is oblate and can be fully characterized through two-dimensional observation along the plane perpendicular to the foliation (Sheridan and Ragan 1976). Viscosity contrasts between constituents control the flow dynamics in these systems. Mass transfer flow is thus expected to play a fundamental role in strain accommodation. The very high viscosity differences between melt and particles allows modeling of flow as a matrix (melt) undergoing ductile deformation embedding perfectly rigid solid particles such as crystals and lithic fragments. Magmatic deformation is marked by well-developed strain fabric of the liquid matrix with crystals generally unaffected by strain; this occurs when the crystal content is lower than 55% in volume, and particles dispersed in the fluid can rotate under the influence of the shear stress (Arzi 1978; Van der Molen and Paterson 1979). At low crystal concentration, crystal-preferred orientation, rotating structures around crystals, as well as asymmetric folds and inclined vesicles and shard textures, are indicative of magmatic flow and can be used as kinematic indicators (Nicolas 1991; Vernon 1987; Blumenfeld and Bouchez 1988; Passchier and Simpson 1986) to determine the direction and sense of shear.

Geologic setting

The Nuraxi Tuff is a Miocene, high-grade, lithic-poor, rhyolitic ignimbrite erupted about 15.8 Ma in the Sulcis volcanic district (SW Sardinia, Italy, Fig. 1). It is dispersed over an area of about 700 km², and is part of an up-to-200 m-thick succession of 11 calc-alkaline to peralkaline, dacitic to rhyolitic ignimbrites (Assorgia et al. 1990; Morra et al. 1994; Pioli 2003) erupted between 17.6 and 13.8 Ma. These ignimbrites were emplaced in the southern portion of the magmatic arc that crossed western Sardinia during the main phase of the opening of the Western Mediterranean basin and the Apennine subduction (Beccaluva et al. 1985; Dostal et al. 1982; Vigliotti and Langenheim 1995).

Fig. 1 Geological map of the Sulcis volcanic basin and location of sampling sites



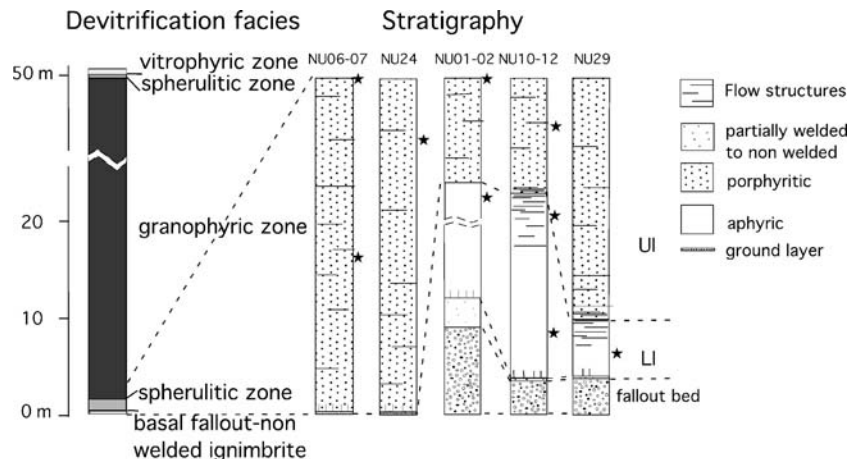
Moderate posteruptive deformation of the volcanic succession occurred as vertical faulting with maximum downthrow of 40 m. This faulting also led to partial marine submergence of the Sulcis basin and the formation of S. Antioco and S. Pietro islands (Fig. 1).

The ignimbrite was emplaced in diverse topographic settings: these include a 10 km² plateau in the northern part of the Sulcis District (near Portoscuso), a N–S trending depression on western S. Antioco Island, and isolated paleo-topographic highs near M. Pranu lake. The Nuraxi Tuff consists of two units (Lower Ignimbrite, LI, and Upper Ignimbrite, UI) distinguished by different crystal contents and aerial distributions (Fig. 2) described in detail by Pioli and Rosi (2005). Although the vent of the ignimbrite is not exposed, distribution of welding and devitrification facies as well as mesoscale structures indicate a source area to the northwest of the Sulcis coast (Pioli and Rosi 2005).

Welding fabric of the Nuraxi Tuff

The Nuraxi Tuff is remarkably foliated and variably rheomorphic. Parataxitic texture, defined by prolate fiamme oriented with the main axis and flow features, are widespread along the whole thickness. Horizontal foliation, local gentle folding and clear parataxitic texture are common features in the Sulcis area where paleotopography was flat at the time of the current emplacement, whereas intensely rheomorphic, flow-banded and folded facies occur mostly in S. Antioco and S. Pietro Island paleo-valleys. The tuff displays a regular association of flow facies in most of the outcrops, showing a basal massive layer (0.5–1.5 m), upward gradually increasing intensity of deformation up to intensely flow-layered facies (1–4 m, thickness varying with local paleotopography and thickness of LI), followed by foliated, parataxitic facies.

Fig. 2 Simplified stratigraphic columns of the Nuraxi Tuff in the studied area. Stars indicate positions of layers sampled for magnetic studies



Micro-scale flow features are particularly well preserved in the LI, in which the vitroclastic texture was not obliterated by granophytic crystallization of the matrix. Rheomorphic features include elongated cavities, micro-scale folds and rotational structures in the matrix around crystals and lithic fragments. The matrix of the tuff consists of highly deformed shards whose aspect ratio is generally lower along the plane parallel to lineation and perpendicular to foliation. Deformation of the matrix around rigid particles is not uniform and microfolds involving sub-millimeter to several centimeter-thick layers occur in the higher strained facies. The microfolds are generally enclosed between discontinuities that likely represented sliding surfaces during the flow. In intensely rheomorphic facies, asymmetrical deformation structures in the matrix occur around the majority of crystals (up to 90%). In the main body of the tuff, micro-scale features are obliterated by extensive devitrification of the matrix except in the basal and top layers, which are only mildly affected by spherulitic crystallization. Mesoscopic flow directions measured in sites distributed throughout the basin indicate that flow was primarily laminar and from NW to SE in the Cortoghiana plateau (Pioli and Rosi 2005). In other localities, mainly in S. Antioco and S. Pietro islands, rheomorphic features indicate a complex, multiphase, laterally discontinuous deformation produced by slumping of discrete layers along dipping surfaces. The structural features, the zoning of welding facies, and vertical density profiles suggest that the welding process was relatively independent of lithostatic load and was instead controlled by extensive particle agglutination and rheomorphic flow in the pyroclastic density current (Pioli and Rosi 2005).

Sampling and measurements

The 29 sampled outcrops are evenly distributed across the exposure area of the Nuraxi Tuff (Figs. 1 and 2) and mainly located in the lower 2 m of the welded ignimbrite. At each site, we measured the orientation of the foliation plane, the lineation and the sense of flow as inferred from mesoscale flow markers, together with the stratigraphic height from the base level of the tuff, if exposed (Table 1). Samples for AMS measurements were typically collected in small groups of 8–12 cores a few cm apart from each other along the same layer or height above the base. This style of sampling is designed to ensure that we analyze specimens that were deposited under nearly the same conditions at about the same time. Two or three layers at different stratigraphic heights were sampled at sites 1–2, 6–7, 10–11–12, 27–28. At Portoscuso, we sampled nine distinct layers (sites 13 to 21) throughout the ≈ 8 m thick section. Samples were collected either by hand or using a gasoline-

powered drill, oriented with both magnetic and solar compasses, and then cut in the laboratory to standard cylindrical specimens. Magnetic measurements were done at the paleomagnetic laboratories at the University of California at Santa Barbara (USA) and at the Alpine Laboratory of Paleomagnetism (ALP; Torino, Italy).

We also carried out a study of the mesoscopic to microscopic flow features of the rock in a selected area, located close to Cortoghiana, and compared this to AMS on the same samples. Micro-structural analyses of flow facies and micro-scale observation were concentrated in the layers of the tuff where vitroclastic texture is preserved; in particular we selected a well-exposed, laterally continuous, representative section to compare magnetic and petrofabric studies in the Sulcis area (sites NU10–NU12). Besides AMS measurements, crystal concentration, crystal shape distribution and orientation, vesicle shape, geometry and concentration of rotation structures around crystals were measured in oriented thin sections cut from hand samples from different stratigraphic heights. Scanning electron microscopy observations (SEM) and SEM–Energy-dispersive X-ray spectroscopy (EDS) analyses were also performed on the same samples to characterize the magnetic mineralogy and its distribution throughout the ignimbrite.

Results

Magnetic mineralogy

Some specimens from different locations and facies were first given an isothermal remanent magnetization (IRM) and then thermally demagnetized according to the Lowrie (1990) method. NRM was measured using an AGICO jr-5 spinner magnetometer. This allows the discrimination of the relative contribution of the different magnetic carriers occurring in the rock, and the identification of the minerals that actually control the magnetic properties of the rock. The results demonstrate that samples have a dominant fraction of low coercivity minerals (Fig. 3). Thermal demagnetization shows that the IRM components gradually decrease to zero at temperatures between 520°C and 570°C. Unblocking temperatures are similar in all samples. These results show that low coercivity Ti-magnetite is the main ferromagnetic mineral in the Nuraxi Tuff. Petrographic observations reveal that Fe-oxide microphenocrysts represent less than 1% by volume in LI and about 1% in the UI. Their dimensions range from 150 μm to 1 mm. Compositions of the crystals were investigated using SEM–EDS techniques on a Philips XL30 SEM equipped with EDAX X-41. The spectra obtained show the occurrence of both ilmenite and low Ti-magnetite crystals. Opaque microlites occur in the matrix of the tuff, their dimension and

Table 1 Stratigraphic position, mesoscale structural data, bulk susceptibility, directions of the maximum (k_1) and minimum (k_3) anisotropy axes and main AMS parameters of all the sampling sites of Nuraxi ignimbrite

Site	Number	Unit	Stratigraphic height (m)	k_1		k_3		P (X_1/X_3)	T	Type	Bulk susc. (μ S.I.)	Average density (kg/m^3)	Structural foliation (pole)		Structural lineation	
				D	I	D	I						D	I		
NU01	6	LI	M	0.80	275	67	163	10	1.012	0.287	3	4,975	2,529	(216	84)	(*90)
NU02	10	UI	L	4.50	280	6	75	83	1.018	-0.124	1	11,112	2,508	156	10	*90
NU03	12	UI	L	2.00	294	10	83	79	1.014	-0.056	1	1,643	2,429	10	84	*123
NU04	14	LI	L	0.60	312	17	115	73	1.042	-0.418	1	6,952	2,321	10	82	132
NU05	8	UI	M	-	139	30	234	7	1.008	0.365	4	396	1,963	(190	80)	-
NU06	9	UI	L	1.00	331	2	233	77	1.024	-0.461	1	3,101	2,391	230	87	*140
NU07	3	UI	L	4.70	324	5	67	68	1.017	-0.318	1	4,348	2,413	230	87	*140
NU08	10	LI	M	0.32	180	10	10	80	1.033	0.719	3	12,313	2,300	(298	87)	(*56)
NU09	13	UI	L	1.03	219	19	26	71	1.058	0.153	1	10,534	2,343	(298	87)	*56
NU10	11	LI	L	0.60	312	13	86	72	1.062	-0.174	1	6,148	2,288	80	85	125
NU11	11	UI	L	0.88	310	23	77	55	1.046	-0.746	1	14,343	2,338	80	85	125
NU12	2	LI	M	0.40	-	-	-	-	1.045	0.704	3	7,659	-	(72	80)	(125)
NU13	21	LI	L	0.53	293	8	116	82	1.052	-0.297	1	7,248	2,183	270	90	119
NU14	20	UI	L	0.90	293	16	171	62	1.091	-0.822	2	6,931	2,143	270	90	119
NU15	10	LI	M	0.27	31	2	161	87	1.038	0.649	3	9,842	2,511	(270	90)	(119)
NU16	12	UI	L	1.58	296	28	170	48	1.023	-0.309	1	3,791	2,253	270	90	119
NU17	10	UI	L	2.15	302	12	178	70	1.020	-0.385	2	4,428	2,293	270	90	119
NU18	18	UI	L	4.22	295	19	134	70	1.019	0.096	1	4,178	2,274	270	90	119
NU19	17	UI	L	5.32	297	10	169	74	1.018	0.004	1	5,293	2,349	270	90	119
NU20	15	UI	L	6.40	294	19	136	70	1.015	0.045	1	5,553	2,370	270	90	119
NU21	18	UI	L	7.20	295	18	162	64	1.015	0.082	1	5,408	2,231	270	90	119
NU22	13	UI	L	1.60	279	13	106	77	1.056	-0.739	2	9,378	2,244	132	84	*280
NU23	14	UI	L	top	261	5	3	65	1.052	-0.184	1	3,642	2,325	146	87	245
NU24	8	UI	L	1.50	165	17	349	73	1.013	-0.099	1	10,011	2,527	60	87	344
NU25	10	UI	M	2.00	310	10	118	79	1.004	-0.030	4	571	2,154	-	-	-
NU26	16	UI	L	1.05	233	1	324	30	1.034	-0.869	2	9,476	2,285	10	75	252
NU27	14	UI	L	rheom	291	0	20	51	1.026	0.167	1	7,461	2,334	4	6	*100
NU28	14	UI	L	rheom	280	7	190	1	1.039	-0.335	1	6,156	2,272	4	6	*100
NU29	13	LI	M	0.35	36	2	144	83	1.008	0.402	3	4,811	2,268	(168	80)	(290)

L linedated facies *M* massive facies. Massive facies: Foliation planes and structural lineations are enclosed in brackets and refer to basal contact orientation and lineation as measured in upper layers, same outcrops, respectively. Structural lineation data refer to flow azimuth, as inferred from flow indicators, unless preceded by an asterisk, where refer to pure lineation direction

distribution varying with crystallization zones of the ignimbrite. In detail, the top vitrophyric facies has widespread elongate opaque microlites ($\leq 5 \mu\text{m}$ long); qualitative EDS analyses of the grains, with main peaks

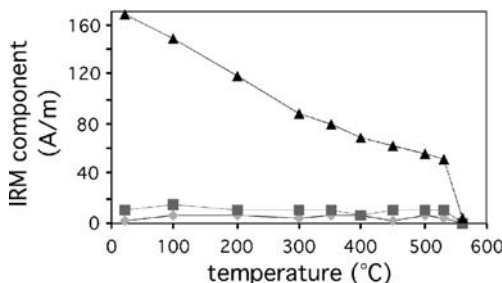
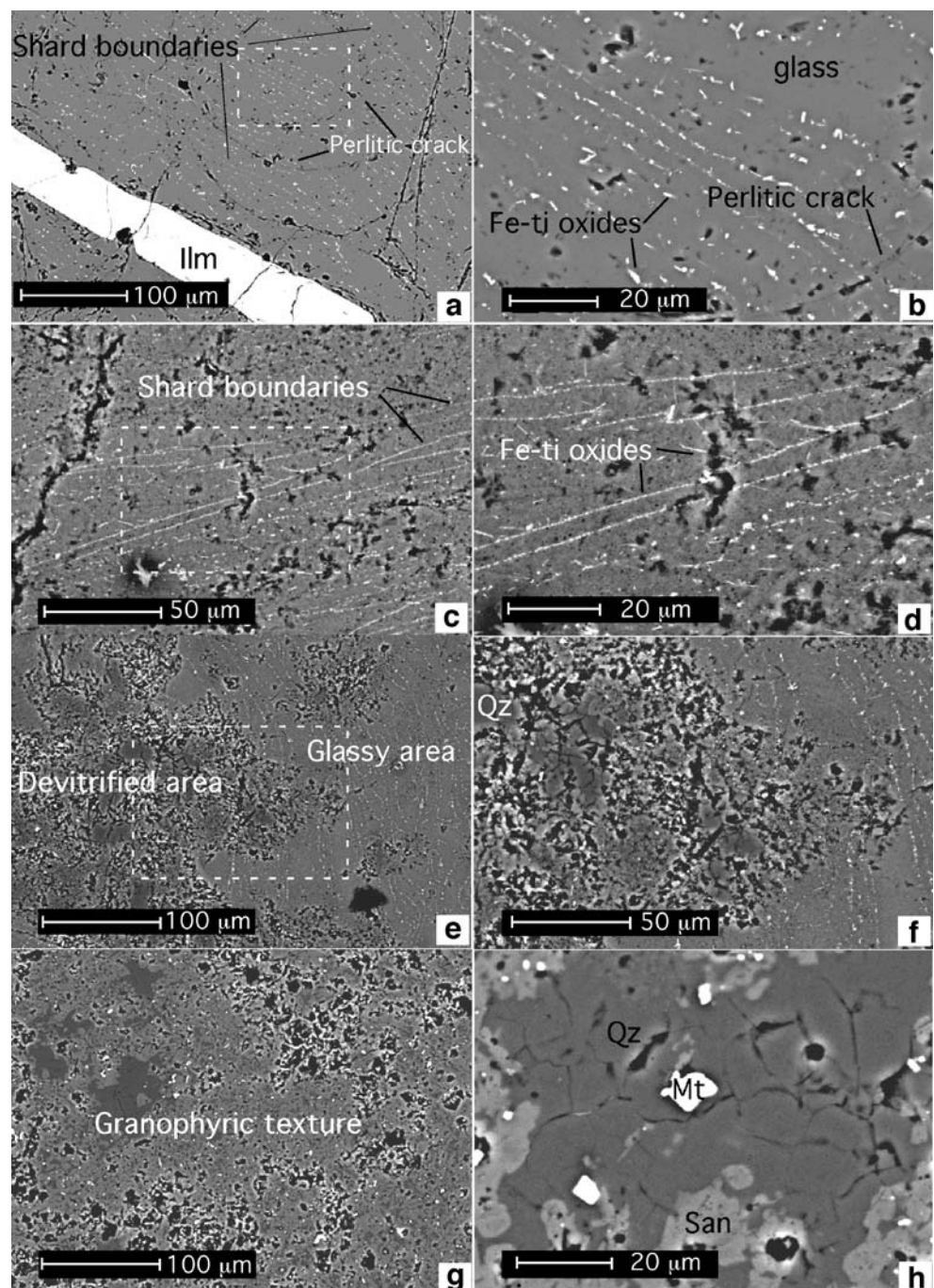


Fig. 3 Thermal demagnetization of three-component IRM of specimen NU11e from Nuraxi Tuff. *Triangles, squares and diamonds* indicate the low-, intermediate-, high-coercivity component, respectively

for O, Fe, Ti, and minor peaks for Si, Al and Mg, indicate that these crystals are Fe–Ti oxides. Most of the grains are in contact and form elongate trails that mimic shard morphologies (Fig. 4a, b). These trails parallel the welding fabric and mark the contact between deformed shards; the bands are widespread and their occurrence, thickness, and distribution are not affected by perlitic cracks in the glass or local spherulitic nuclei. This uniformity suggests that they formed very early, possibly just after emplacement, and are not related to alteration processes. Other grains are scattered in larger shards and lapilli (Fig. 4c, d). Granophyric crystallization obliterates primary structures (Fig. 4e, f) replacing the microlite trails and glass by silica and sanidine aggregates and large (10–15 μm) Fe-oxide microlites. Distribution of minerals in the devitrified zones is homogenous with no traces of individual shards preserved (Fig. 4g, h).

Fig. 4 SEM-backscattered images from thin sections of densely welded facies of the Nuraxi Tuff. **(a)** UI upper vitrophyric facies; vitroclastic texture is outlined by microlites marking shard boundaries **(b)** Higher magnification image of the area enclosed in **(a)**; showing elongated Fe-oxide microlites aligned into discrete bands **(c)** UI, specimen NU13e, spherulitic facies. Cryptocrystalline matrix showing vitroclastic texture highlighted by microlite trails marking shard boundaries; **(d)** higher magnification image of area enclosed in **(a)**; and **(e)** and **(f)** Variably crystallized matrix of the UI tuff in specimen NU08f; *granophyric patches* on the left-side of picture **(e)**, enlarged in picture **(f)**, interrupt vitroclastic texture preserved in cryptocrystalline tuff; **(g)** and **(h)** UI, specimen NU16a; granophyric facies: the matrix consists of sanidine, silica and Ti-magnetite aggregates



Natural remanent magnetization

Natural remanent magnetization (NRM) was measured on a few cores from each site. The results were broadly similar and a more complete study of remanence characteristic was only done at eight sites. The specimens were stepwise demagnetized either thermally (20–610°C) or in an alternating field (0–100 mT). Susceptibility was measured after each heating step to check for possible mineralogical transformations, and never changed significantly. Blocking temperatures were nearly always lower than 600°C and

consistent with the widespread occurrence of Ti-magnetite. Only site NU05 (non-welded tuff) had more than 80% of the initial NRM survive heating to 610°C. This result is consistent with petrographic observations of non-welded tuff samples, which reveal extensive devitrification of fiamme and matrix and alteration of phenocrysts, and the minor occurrence of hematite. Significant secondary components were present in samples from all sites, as shown by the high dispersion of the NRM mean site direction ($4.3^\circ \leq \alpha_{95} \leq 20.5^\circ$). These components were easily removed by thermal demagnetization at temperatures below 300°C

Fig. 5 Orthogonal plots of thermal demagnetization results and normalized remanence intensity curves of two representative cores. *Solid and open symbols in orthogonal plots* represent projections on horizontal and vertical planes, respectively

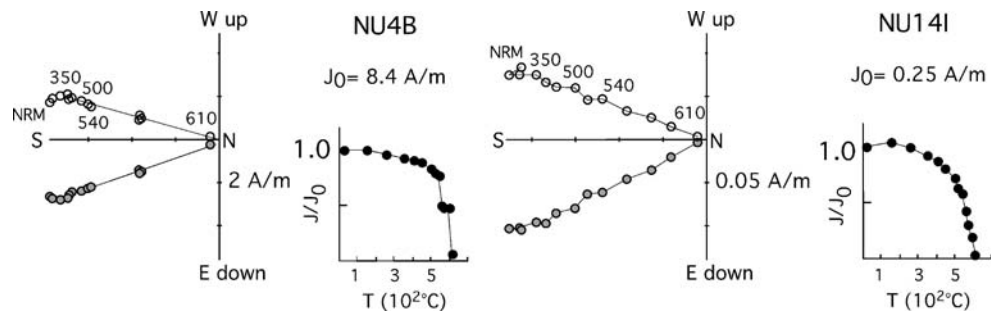


(Fig. 5). The characteristic remanent magnetization (ChRM) directions (Table 2) have a very small dispersion both within ($1.6^\circ \leq \alpha_{95} \leq 6.1^\circ$), and between ($\alpha_{95} = 4.5^\circ$) sites. The consistency of the ChRM directions throughout all of the sampling region shows that the Nuraxi Tuff did not undergo any significant movement after the acquisition of its remanence.

Magnetic fabric

Low-field magnetic susceptibility and its anisotropy were measured on a total of 356 specimens. The site mean values of the principal directions (maximum k_1 , intermediate k_2 , minimum k_3) were calculated using the Jelinek (1978) statistics, and the bulk susceptibility and the main anisotropy parameters calculated as arithmetic means. They are reported in Table 1, together with density, stratigraphic height and mesoscale structural data of each sampling site. Bulk susceptibility shows no relation to the density, which varies from 2,100 to 2,500 kg/m³, nor to the phenocryst content. The average susceptibility of the specimens from the crystal-poor LI is $8,712 \pm 2,312 \mu\text{SI}$ and that of the specimens from the crystal-rich UI is $6,097 \pm 3,192 \mu\text{SI}$. On the other hand, bulk susceptibility varies systematically over a little more than one order of magnitude as a function of the facies. The susceptibility values of the partially devitrified vitrophyre facies (3,000–14,300 μSI), including the basal meter of the deposit, are higher on average than

those of the devitrified facies (1,000–4,500 μSI ; Fig. 6a), and the non-welded, distal facies displays the lowest susceptibility values (<600 μSI). Variability of bulk susceptibility in the welded facies indicates that it is mainly affected by post-depositional crystallization processes. Lower temperature granophyric crystallization of low susceptibility minerals, such as feldspars and quartz, extensively replaced the glassy matrix and most of the small Fe–Ti oxide grains in the main body of the ignimbrite. This crystallization obliterated vitroclastic textures and significantly lowered bulk susceptibility.

The degree of anisotropy ($P = k_1/k_3$) is generally very low ($1.02 < P < 1.06$), higher than 1.05 at only six sites. Foliation ($F = k_2/k_3$) is very weak, with a main mode at 1.01 (Table 1, Fig. 6b) and generally lower than lineation ($L = k_1/k_2$), which shows three peaks centered at 1.01, 1.03 and 1.06. The shape of the AMS ellipsoid, as defined by the Jelinek’s parameter T (Jelinek 1981), is variable from prolate to oblate; T ranges between -0.869 and 0.719 with the main mode centered at zero.

In spite of the weak anisotropy, the magnetic fabric is well developed and can be grouped into four distinct types (Fig. 7):

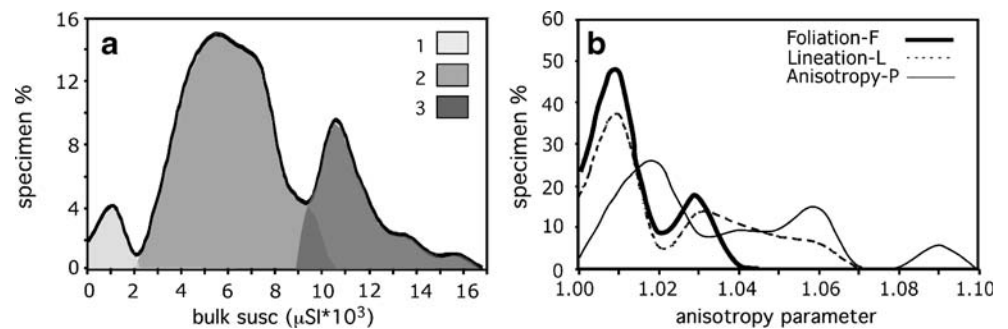
Type 1. All the principal directions ($k_1 > k_2 > k_3$) are tightly grouped and k_3 is nearly vertical. The magnetic foliation plane is close to the horizontal (<20°) and the magnetic lineation is clearly defined. This

Table 2 Mean site NRM and ChRM directions of selected sites from Nuraxi ignimbrite

Site	Number	Unit	NRM		α_{95}	ChRM		α_{95}
			D	I		D	I	
NU04	7	LI	120	15	16.2	161	-16	2.6
NU11	5	UI	121	5	20.5	156	-21	6.1
NU16	5	UI	170	-9	15.8	166	-19	2.5
NU19	5	UI	154	-11	4.3	162	-18	3.0
NU22	7	UI	152	-20	13.6	151	-21	4.0
NU27	7	UI	121	33	17.2	167	-17	3.2
NU28	7	UI	185	-31	16.6	166	-18	4.7
NU29	9	LI	192	-25	8.5	172	-21	1.6

N number of specimens, *D* declination, *I* inclination; α_{95} 95% semi-angle of confidence

Fig. 6 **a** Distribution of the bulk susceptibility of analyzed specimens. 1 non-welded facies 2 granophytic and spherulitic facies 3 vitrophyric and spherulitic facies. **b** Distribution of degree of anisotropy (P), foliation (F), and lineation (L)



type includes most of the sites (18) from both LI and UI units, and corresponds to slightly rheomorphic, parataxitic ignimbrite.

- Type 2. The k_1 directions are again tightly grouped, whereas k_2 and k_3 form a girdle along a plane. The fabric is thus strongly lineated and the foliation plane is poorly defined. These sites ($n=4$) comprise intensely rheomorphic, strongly lineated facies of both units, with abundant micro- to mesoscale flow features.
- Type 3. The k_3 directions are well grouped and vertical; k_1 and k_2 are moderately dispersed within the foliation plane. These five sites were sampled from massive basal LI. This looks like a typical ‘ignimbrite’ fabric (Tarling and Hrouda 1993).
- Type 4. The principal directions are dispersed, the degree of anisotropy is very low and the fabric is poorly defined. Bulk susceptibility is also very low (less than 1,000 μSI). The only two sites of this type

represent non-welded ignimbrite and massive ignimbrite sampled from distal locations. It is also a common type in most ignimbrites (Fisher et al. 1993; Le Pennec et al. 1998).

The AMS data from type 1 and 2 sites can be used as a proxy for the flow direction. The k_1 directions are close to lineations measured in the field (Table 1, Fig. 8) and generally plunge upflow. Large shifts (on average around 20°) occur between k_3 and structural foliation planes for type 1 and 2 sites. In type 1 sites, magnetic foliation plunges upflow and the angle between the magnetic and meso-structural foliation is typically less than 25° ; larger angles up to 51° occur only in three cases; in contrast, compaction seems to dominate type 3 sites, where the fabric is strongly oblate ($0.287 \leq T \leq 0.719$) and the k_1 directions are up to 90° off the lineation measured in the field.

Interpretation of the AMS in terms of rock fabric requires a deeper understanding of its sources. In rocks containing Ti-magnetite, the magnetic lineation may result from either shape or distribution anisotropy. Distribution anisotropy is due to the regular alignment of grains close enough to magnetically interact with each other, as seen in the microlite trails shown in Fig. 4b (Stephenson 1994; Cañon-Tapia 1996). The AMS of a single mineral grain can be parallel to or skewed from the mineral’s physical elongation (shape anisotropy). Shape anisotropy depends on both the shape and the state of the Ti-magnetite grains, being different according whether the grain is multi- (MD, including pseudo-single PSD) or single-domain (SD). The k_1 axis, and thus the magnetic lineation, is parallel to the longest dimension of MD grains and to the shortest dimension of SD grains. In order to discriminate between the two possibilities, the anisotropy of isothermal remanent magnetization (AIRM) is used, because the easy direction of remanence matches the longest direction of the grains irrespective of whether they are MD or SD. AIRM was therefore measured on about 20 specimens from different sites. The specimens were first tumbling demagnetized at 60 mT peak-field and then given an IRM with a steady field of 20 mT. The measurements were repeated in 12 different positions and the anisotropy tensor calculated according to

VARIABILITY OF AMS FABRIC

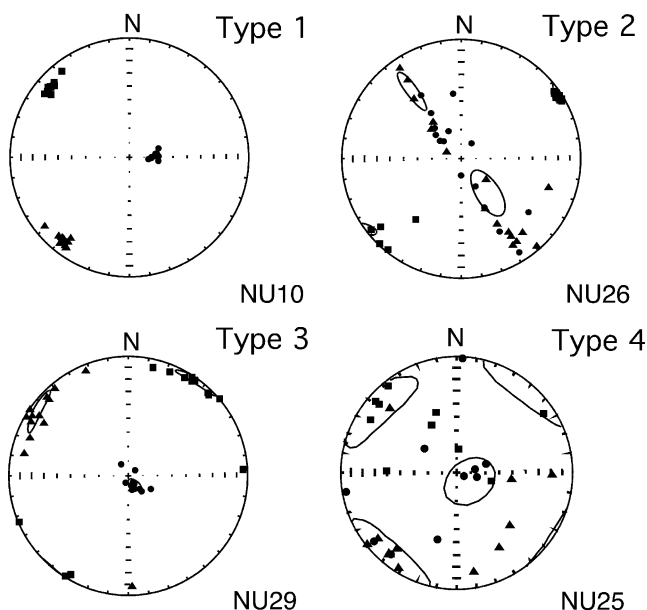
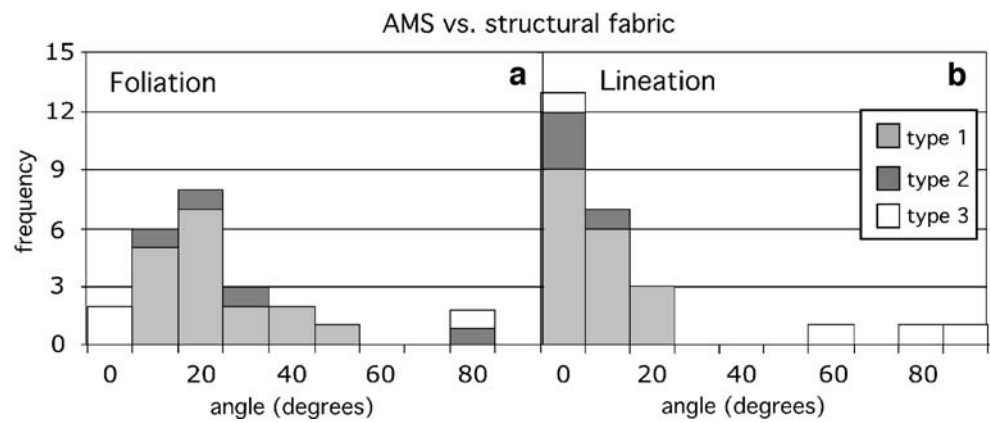


Fig. 7 Lower hemisphere, equal-area projections of the AMS axes ($k_1 > k_2 > k_3$) in the main types of magnetic fabric in Nuraxi Tuff

Fig. 8 Histograms of the distribution of *a* angles between AMS and structural foliation planes and *b* angles between AMS and structural lineation axes for the analyzed sites



the procedure suggested by Jelinek (1978). The orientation of the AIRM ellipsoid is similar to that of the AMS ellipsoid (Fig. 9): the angles between the corresponding axes are always less than 15°. The main difference occurs for the degree of anisotropy, since the AIRM degree $1.044 \leq P_{\text{AIRM}} \leq 2.133$ is larger than the AMS degree, as expected (Stephenson et al. 1986; Potter and Stephenson 1988). These results show that SD grains do not significantly affect the magnetic fabric and that the majority of grains occur as PSD and MD. We can therefore conclude that most of the Ti-magnetite grains in the Nuraxi Tuff are oriented with their longest dimension parallel to the flow direction of the ignimbrite. The AMS k_1 axis corresponds to the average of the long dimension of the magnetic grains.

Strain facies of the basal layers of the tuff in the Cortoghiana area

In the Cortoghiana area, the LI is 76 cm thick and the UI is up to 7 m thick, about 1/5 of the original thickness as inferred from borehole data (Fig. 2; Pioli and Rosi 2005). The LI is densely welded and massive in the lowermost 10 cm. Above this level, the structure is imbricated (shards and vesicles are inclined up to 20° with respect to the basal contact) up to 30 cm from the base. Foliation gradually

increases upward, as well as flattening and stretching of vesicles. Striated plane-parallel partings occur at the top of the LI and within the UI, reaching a minimum spacing (1–2 cm) at the contact between UI and LI. Above this contact, the UI is foliated with a parataxitic texture, and parting planes occur at decimeter intervals. Porosity is minimum at the very base of the deposit, increases upward, and remains constant in the UI, showing no direct relation with the intensity of welding (Pioli and Rosi 2005).

Micro-scale observations revealed further rheomorphic structures and preferred orientation of crystals. Two different types of deformation structures occur in the matrix of LI around crystals and lithic clasts (Fig. 10): (1) *symmetric*: the welding fabric around the grain is deflected and two “tails” depart from the center of the grain at both sides (deformation of the matrix is symmetrical with respect to the plane of the welding foliation); these mostly occur in the thin section perpendicular to the lineation; and (2) *asymmetric*: the welding fabric around the grain is deflected; two tails depart at different heights from the grain, the deformation of the matrix is asymmetrical with respect to the welding foliation plane. Asymmetric structures have been recognized only in thin sections cut parallel to the lineation.

Discussion

Origin of the magnetic fabric

Paleomagnetic data are often useful to further constrain the interpretation of the magnetic fabric results. In our case, for example, the orientation of the petrofabric at some sites is different from the general orientation in the area. The cause of this difference may be primary, as topographic effects linked to the paleosurface, or secondary, associated with tectonics or tilting. Paleomagnetic data help in differentiating the cases. The fact that the ChRM direction does not change from about 350°C up to 610°C bears witness that the NRM was acquired during the tuff emplacement.

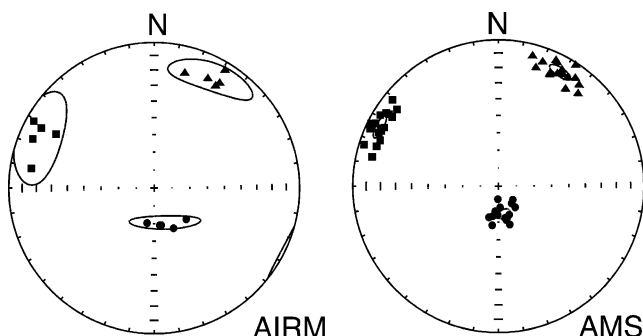
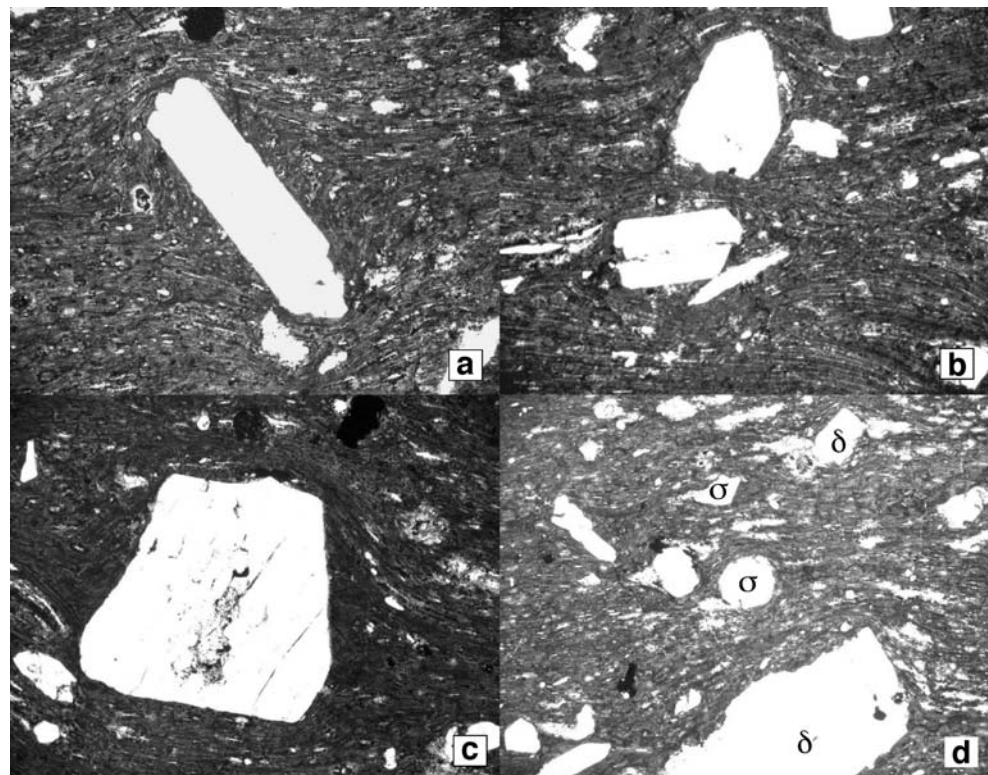


Fig. 9 Lower hemisphere projections of AMS and AIRM axes for site NU19. The 95% confidence interval is outlined in each projection. Squares k_1 , crosses k_2 , circles k_3

Fig. 10 Flow microstructures in vitrophyric facies of the Nuraxi Tuff. **a** δ rotational structure in the matrix around a plagioclase phenocryst **b** rotational structures and broken and displaced phenocryst **c** δ structure around an equidimensional crystal **d** δ and σ structure coexisting in the same layer. σ structures are more common in the matrix around equidimensional crystals



The paleomagnetic direction of the Nuraxi Tuff is $D=162.6$, $I=-19.0$ with $\alpha_{95}=4.5^\circ$. The reverse polarity is consistent with the isotopic age of 15.79 ± 0.16 Ma (Pioli 2003), which falls into the chron 5Br of the GPTS (Cande and Kent 1992) and lasted from 15.155 to 16.014 Ma. On the other hand, the direction does not fully agree with that expected for middle Miocene rocks in Sardinia. Declination is consistent with literature data (Vigliotti and Langenheim 1995; Deino et al. 2001; Speranza et al. 2002), which show that the counter-clockwise rotation of Sardinia with respect to stable Europe was still in progress during middle Miocene time. In contrast, the inclination (19°) is much lower than the values of 40° to 50° expected on the grounds of the Sardinian paleolatitude in Miocene time. The low value of inclination occurs at the sites where NRM was investigated as well as at all other sites, where a few pilot specimens were stepwise demagnetized and yielded fully equivalent results. Explanations such as rheomorphic deformation, compaction, or post-emplacment tilting are hardly tenable because such effects (1) should vary from site to site according to local conditions and (2) would not be large enough to systematically lower the inclination by 20° to 30° within all the Nuraxi Tuff deposits. Anisotropy of remanence would be an attractive explanation because it entails that the remanence vector is deviated toward the easy magnetization axis (Coe 1979; Stephenson et al. 1986). The AMS and AIRM measurements have shown that these axes are close to the horizontal, so that the remanence vector should be less inclined than the Earth's

magnetic field at the time of emplacement. However, the average value of the AIRM anisotropy degree (P_{AIRM}) is 1.13 and could only account for an inclination shallowing of a few degrees (Uyeda et al. 1963). A viable explanation would be that the paleomagnetic direction is transitional. The Nuraxi Tuff might have been emplaced in a short time during either an excursion or transition from the normal polarity chron C5Cn1n and the reverse chron C5Br, which occurred around 16.014 Ma. This hypothesis can be checked by extending the paleomagnetic study to other Miocene ignimbrites of the Sulcis volcanic district.

The Nuraxi Tuff displays both chemical and thermo-remanent magnetization, related to the crystallization of Ti-magnetite grains in the matrix of the tuff at high temperatures, just after deposition. Phenocryst contribution to the fabric is secondary. AMS and AIRM are related to the distribution anisotropy of the grains that crystallized along micro-scale discontinuities in the glassy matrix, primarily in walls of vesicles and on shards surfaces, mimicking external shapes of the deformed particles. The intensity of susceptibility is also affected by late devitrification processes, which likely altered vapor-phase crystals, but no significant change in spatial orientation or geometry of the fabric occurred.

Strain fabric in the basal ignimbrite

Microstructural analyses of vitrophyric facies of the tuff revealed the diffuse occurrence of rotational structures

around phenocrysts (Fig. 10). These structures have a strong analogy with rotational structures occurring around porphyroclasts in mylonites and ultramylonites. By analogy to shear-box experiments results, we believe that such structures form in response to rotation of the grains due to shear flow (Passchier and Simpson 1986). Their geometry is dependent on the geometry of the flow, and the total amount of strain. In analogy with this classification, and based on the geometry of the tails, asymmetric structures were divided into σ and δ types (Passchier and Simpson 1986). A detailed study of δ , σ , rotating structures that occur in the matrix around phenocrysts and lithic particles in LI was performed in order to determine the geometry of the flow (kinematic

vorticity number as defined by Passchier 1987). The geometry and concentration of rotational structures, and the relation between shape and orientation of crystals and rigid inclusions are consistent with prevailing compaction deformation in the lower, massive layer of the ignimbrite, and rapid upward increase of shear strain (Fig. 11a, b). The absence of any relation between the particle aspect ratio, angle between the flow direction and particle main axis, and the type of structure developed (Fig. 11c) indicates that practically all the particles rotated until the flow ceased irrespective of their shape in turn indicating a simple shear regime (Fernandez et al. 1983; Masuda et al. 1995; Gosh and Ramberg 1976; Nicolas 1991).

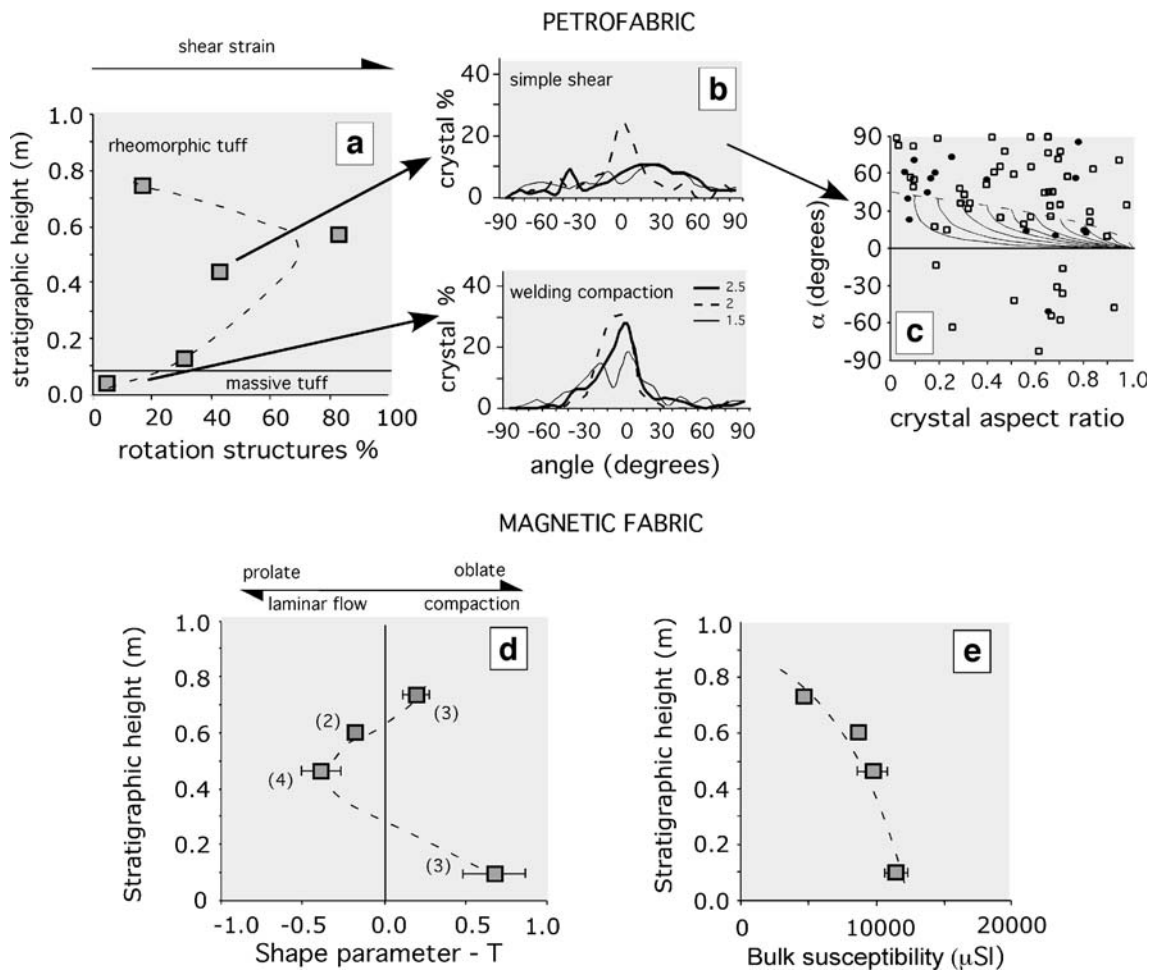


Fig. 11 Main AMS and structural parameters of Portoscuso outcrop. **a** variation of relative concentration of rotation structures in the matrix around crystals; concentration of flow structures is used as a qualitative indicator of finite strain. Variation of percentage of rotational structures accords well with variation of other indicators of finite strain, such as shards, lapilli and vesicle aspect ratio. **b** Histograms of angle between crystal long axes and flow direction in sections parallel to lineation. *Thin line* crystals with aspect ratio 1.5; *thick line* crystals with aspect ratio 2; *dashed line* crystals with aspect ratio 2.5. *Histogram from basal sample* shows preferred orientation of all crystal, irrespective of their shapes, whereas *histogram from upper layers* display shape-sensitive orientation of crystals, demonstrating

prevailing pure and simple shear, respectively (Ježec et al. 1994; Iezzi and Ventura 2002); **c** plot of orientation vs. shape of rotated crystals in section parallel to lineation. *Thin lines* represent the areas of stability of particles in flows with increasing vorticity numbers (k_w ; after Gosh and Ramberg 1976). α is the angle between crystal long axis and shear direction. *Circles* and *squares* indicate sigma and delta rotating structures, respectively, as defined by Passchier (1987); **d** shape of the AMS ellipsoid vs. stratigraphic height **e** Bulk susceptibility vs. stratigraphic height; *number in brackets* refer to number of analyzed specimen in the level; *error bar* refer to whole variability of the parameter in the analyzed specimens

Due to the extreme deformation of the matrix, no flame are visible in the LI, and so it is not possible to calculate the finite strain. An estimation of the minimum lateral displacement of the agglutinated mass during laminar flow in LI can be calculated using Fernandez et al. (1983) 2D-model for preferred orientation of ellipsoidal particles in simple shear deformation, assuming no mechanical interaction between particles and Newtonian behavior of the matrix. Such minimum displacement corresponds to 3 m. We envisage that the actual runout of the non-particulate portion of the pyroclastic current could have been at least one order of magnitude higher, since most of the deformation during flow was likely accommodated in gas-lubricated flow discontinuities now preserved as parting planes (Pioli and Rosi 2005). The extensive devitrification of the matrix, obliterating primary texture, prevented any calculation of total strain for the UI.

Magnetic fabric and strain

A detailed examination of the samples cored from multiple sites at two nearby outcrops located in the Cortoghiana plateau, about 1 km SE of Portoscuso village (sites 13–21 and 10–12), allows a direct evaluation of the relation between microstructures and magnetic fabric. Further cores were drilled from oriented samples collected for microstructural studies (Fig. 11d, e). Results show systematic differences in the main AMS parameters with stratigraphic height in the two different units (Figs. 11 and 12). Specifically, sites from UI are very similar, but significant changes occur in the lowermost 2 m of the tuff. Cores drilled from the base of the tuff, where welding compaction dominates, have oblate fabrics and display no structures related to magmatic flow. The lineation increases upward in LI, and reaches a maximum in the uppermost LI and lower part of UI where AMS ellipsoids become rotational prolate. There is also a relation between anisotropy and concentra-

tion of flow structures in the tuff. The anisotropy is highest in the intensely rheomorphic facies, showing centimeter-spaced parting planes with parallel striae, elongated vesicles and micro-scale folds in the matrix. In LI, where simple shear strain dominates, magnetic lineation is also positively correlated with intensity of deformation as indicated by the concentration of micro-scale flow structures parallel to the flow direction.

Strain fabric and rheomorphic flow

The geometric properties of the magnetic fabric (orientation and shape of the anisotropy ellipsoids) that derive from the orientation of magnetic grains are mainly related to the strain fabric. Other properties (bulk susceptibility, NRM intensity) that depend on the type and concentration of magnetic grains vary with the crystallization facies of the tuff. The flow plane and the direction and sense of flow were determined in the field by analysis of mesoscale flow features at most sites (Table 1). The magnetic fabric and the strain ellipsoid are coaxial and have similar shapes. As previously inferred for other ash-flow tuffs (Baer et al. 1997), the foliation plane is parallel to the flow plane and the imbrication of the k_1 axes indicates the flow direction in the site. Only some foliated (type 3) sites (NU 8, 15 and 29) display anomalous directions. Flow directions on the Cortoghiana plateau indicate radial spreading of the flow from a source located N of San Pietro Island. Flow directions measured in S. Antioco island are more scattered and influenced by local paleotopography, indicating down-slope flow likely due to decoupling of the basal portion of the current from the upper, low-density, particulate flow along paleo-hills ≤ 400 m high (Fig. 13) on the SE part of the island.

The shapes of the AMS ellipsoids in the Nuraxi ignimbrite vary with stratigraphic height within an individual site. We interpret the lack of structures in the lower

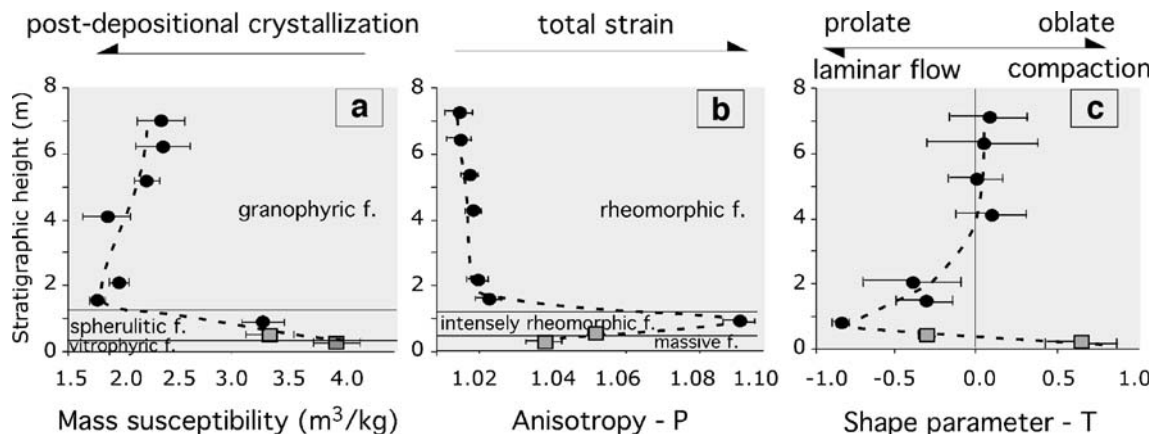
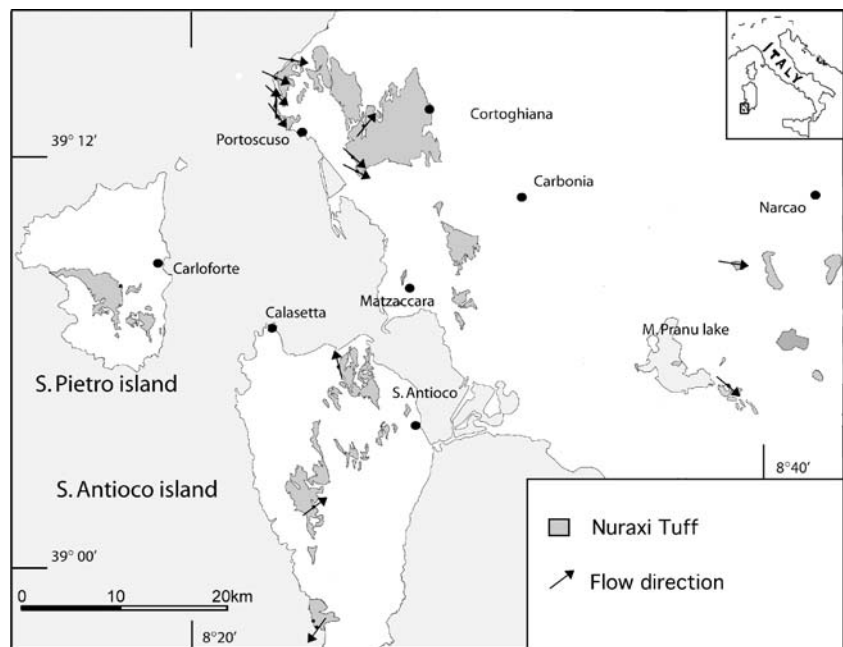


Fig. 12 Variation of the main AMS parameters with stratigraphic height in the E Portoscuso outcrop (sites NU13–NU21). **a** Mass susceptibility, **b** degree of anisotropy (P) **c** shape of the ellipsoid (T). Circles and squares refer to UI and LI sites, respectively

Fig. 13 Map showing mean flow directions as inferred from the orientation of AMS ellipsoids



50 cm of the tuff to result from welding compaction, and the fabric is rotational-oblate (type 3 ellipsoids). The occurrence and geometry of rheomorphic features within the upper layers of the tuff indicate simple shear (laminar flow). Most of the sites sampled from this facies have $T \leq 0$ and the lineation intensity that is positively correlated with the density of meso- to micro-scale flow structures occurring in the tuff, which in turn reflect the duration and extent of rheomorphic flow. Type 1 ellipsoids are typical of the main body of the tuff and type 2 ellipsoids are displayed by the sites cored from intensely rheomorphic facies (Fig. 9) exhibiting prolate strain. The distribution of structures and welding facies indicate that rheomorphic flow occurred at the base of the pyroclastic density current resulting from catastrophic agglutination of pyroclasts in the lower, high concentration part of the non-particulate current (Pioli and Rosi 2005). Magnetic and structural data indicate that the formation of the basal rheomorphic flow occurred after insulation of the current from the substrate due to deposition of a few tens of centimeter of welded tuff (type 3 fabric). The increase in shear strain occurring at the interface between UI and LI could be due to an increase in velocity (carrying capacity) of the pyroclastic current that could have significantly increased thickness and velocity gradient of the basal non-particulate flow, as at this same height we also observe an abrupt coarsening of the deposit.

Samples from sites NU27 and 28 were taken from rheomorphic ignimbrite that slid along the eastern margin of a paleo-valley after deposition (more detailed data about the geometry of the flow are shown in Pioli and Rosi 2005). Samples were cored from two sides of an acute fold with meter-scale wavelength and involving a several-meters-thick

layer of the tuff; they show type 1 ellipsoids displaying orientations that are not representative of the syndepositional flow direction but reflect the mesoscale structures formed during secondary flow. Since the ChRM directions of the cores are not significantly different from the other sites (Table 2), we also argue that these movements ended well before the temperature of the tuff dropped below the Curie point.

Conclusions

Groundmass magnetic minerals, whose distribution reflects existing fabric elements within the tuff, mainly control the magnetic fabric of the Nuraxi ignimbrite. This magnetic fabric results from the distribution anisotropy of micrometer-size grains reflecting the combined effects of primary flow lineation, welding and rheomorphism. Magnetic fabric was acquired during high-temperature crystallization in the glass along discontinuities such as boundaries of shards and collapsed vesicles walls in pumice fragments, mimicking vitroclastic texture. Since the shape of pyroclasts in the deposit is strictly influenced by welding and flow processes (Sheridan and Ragan 1976; Quane and Russell 2005; Russell and Quane 2005), the magnetic fabric, which is a function of the distribution and concentration of the grains, accurately describes the strain fabric of the rock. The shape of the AMS ellipsoid in Nuraxi Tuff samples can be used as an indicator for the rheomorphic flow stage and the intensity of the lineation is directly proportional to the extent of the flow. We also infer that, in the Nuraxi tuff, the shape of the ellipsoid can be used as a qualitative indicator of the relative

importance of compaction vs. rheomorphic flow in the tuff. Similar textures have been described in other tuffs (Hargraves et al. 1991; Thomas et al. 1992; Palmer and MacDonald 1999), and observed by the authors in several welded tuffs, suggesting that distribution anisotropy of secondary magnetite grains is a main factor controlling the magnetic fabric of welded pyroclastic rocks.

Acknowledgements We wish to thank to C. Anderson for hospitality and extensive help during laboratory activities in Santa Barbara; Nancy and Marisa for hospitality in Flagstaff, AZ, USA; F. Mazzarini for fruitful discussions. L.P. was partially funded by a Dipartimento di Scienze della Terra, Università di Pisa research grant. Analysis of paleomagnetic data was performed using Paleomac (J.P. Cogné 2003, *Geochem Geophys Geosyst* 4, 1007). K. Cashman is acknowledged for revision of an earlier version of the manuscript. The paper greatly benefited from detailed and thoughtful revisions by A. Grunder and E. Cañon-Tapia.

References

- Arzi AA (1978) Critical phenomena in the rheology of partially melted rocks. *Tectonophysics* 44:143–169
- Assorgia A, Fadda A, Torrente DG, Morra V, Ottelli L, Secchi FA (1990) Le successioni ignimbritiche terziarie del Sulcis (Sardegna Sud-Occidentale). *Mem Soc Geol It* 45:951–963
- Baer EM, Fisher RV, Fuller M, Valentine G (1997) Turbulent transport and deposition of the Ito pyroclastic flow: determinations using anisotropy of magnetic susceptibility. *J Geophys Res* 102:22565–22586
- Beccaluva L, Civetta L, Macciotta G, Ricci CA (1985) Geochronology in Sardinia: results and problems. *Rend Soc It Min Petrol* 40:57–72
- Blumenfeld P, Bouchez JL (1988) Shear criteria in granite and migmatite deformed in the magmatic and solid states. *J Struct Geol* 10:361–372
- Borradaile GJ, Henry B (1997) Tectonic applications of magnetic susceptibility and its anisotropy. *Earth Sci Rev* 42:49–93 DOI 10.1016/S0012-8252(96)00044-X
- Cande SC, Kent DV (1992) Revised calibration of the geomagnetic polarity time scale for the late Cretaceous and Cenozoic. *J Geophys Res* 100:6093–6095
- Cañon-Tapia E (1996) Single grain versus distribution anisotropy: a simple three-dimensional model. *Phys Earth Planet Int* 94:149–158
- Coe RS (1979) The effect of shape anisotropy on TRM direction. *Geophys J R Astron Soc* 56:369–383
- Deino A, Gattacceca J, Rizzo R, Montanari A (2001) $^{40}\text{Ar}/^{39}\text{Ar}$ dating and Paleomagnetism of the Miocene volcanic succession of Monte Furrù (Western Sardinia); implications for the rotation history of the Corsica–Sardinia microplate. *Geophys Res Lett* 28:3373–3376 DOI 10.1029/2001GL012941
- Dostal J, Coulon C, Dupuy C (1982) Cainozoic andesitic rocks of Sardinia (Italy). In: Thorpe RS *Andesites*. Wiley, London, pp 353–369
- Elwood BB (1982) Estimates of flow direction for calc-alkaline welded tuffs and paleomagnetic data reliability from anisotropy of magnetic susceptibility measurements: central San Juan mountains, southwest Colorado. *Earth Planet Sci Lett* 59:303–314
- Fernandez A, Feybesse JL, Mezure JF (1983) Theoretical and experimental study of fabrics developed by different shaped markers in two-dimensional simple shear. *Bull Soc géol France* 25:319–326
- Fisher RV, Orsi G, Ort M, Heiken G (1993) Mobility of a large-volume pyroclastic flow-emplacment of the Campanian ignimbrite, Italy. *J Volcanol Geoth Res* 56:205–220
- Gosh SK, Ramberg H (1976) Reorientation of inclusions by combination of pure and simple shear. *Tectonophysics* 34:1–70
- Hargraves RB, Johnson D, Chan CY (1991) Distribution anisotropy: the cause of AMS in igneous rocks. *Geophys Res Lett* 18:2193–2196
- Herrero-Bervera E, Walker GPL, Cañon-Tapia E, Garcia MO (2001) Magnetic fabric and inferred flow directions of dykes, cone sheets and sills swarms, Isle of Skye, Scotland. *J Volcanol Geotherm Res* 106:195–200 DOI 10.1016/S0377-0273(00)00293-6
- Hrouda F (1982) Magnetic anisotropy of rocks and its application in geology and geophysics. *Geophys Surv* 5:37–82
- Iezzi G, Ventura G (2002) Crystal fabric evolution in lava flows, results from numerical simulations. *Earth Planet Sci Lett* 200:33–46 DOI 10.1016/S0012-821X(02)00617-9
- Jackson M, Tauxe L (1991) Anisotropy of magnetic susceptibility and remanence: developments in the characterization of tectonic, sedimentary and igneous fabrics. *Rev Geophys Suppl* 29:371–376
- Jelinek V (1978) Statistical processing of anisotropy of magnetic susceptibility measured on groups of specimens. *Studia Geophys Geod* 22:50–62
- Jelinek V (1981) Characterization of the magnetic fabric of rocks. *Tectonophysics* 79:T63–T67
- Ježec J, Melka R, Schulmann K, Venera Z (1994) The behaviour of rigid triaxial ellipsoidal particles in viscous flows—modeling of fabric evolution in a multiparticle system. *Tectonophysics* 229:165–180
- Knight MD, Walker GPL (1986) Stratigraphy, paleomagnetism, and magnetic fabric of the Toba tuffs: constraints on the sources and eruptive styles. *J Geophys Res* 91:10355–10382
- Le Penec JL, Chen Y, Ciot H, Froger JL, Gourgaud A (1998) Interpretation of anisotropy of magnetic susceptibility fabric of ignimbrites in terms of kinematic and sedimentological mechanisms: an anatolian case study. *Earth Planet Sci Lett* 157:105–127 DOI 10.1016/S0012-821x(97)00215-X
- Lowrie W (1990) Identification of ferromagnetic minerals in a rock by coercivity and unblocking temperature properties. *Geophys Res Lett* 17:159–162
- Masuda T, Michibayashi K, Ohta H (1995) Shape preferred orientation of rigid particles in a viscous matrix: reevaluation to determine kinematic parameters. *J Struct Geol* 17:115–129
- Morra V, Secchi A, Assorgia A (1994) Petrogenetic significance of peralkaline rocks from Cenozoic calc-alkaline volcanism from SW Sardinia, Italy. *Chem Geol* 118:109–142
- Nicolas A (1991) Kinematics of magmatic rocks with special reference to gabbros. *J Geol* 33:891–915
- Passchier C (1987) Stable positions of rigid objects in a non-coaxial flow—a study in vorticity analysis. *J Struct Geol* 9:679–690
- Ort MH, Orsi G, Pappalardo L, Fisher RV (2003) anisotropy of magnetic susceptibility studies of depositional processes in the Campanian Ignimbrite, Italy. *Bull Volcanol* 65:55–72 DOI 10.1007/s00445-002-0241-2
- Passchier C, Simpson C (1986) Porphyroclast systems as kinematic indicators. *J Struct Geol* 8:831–843
- Palmer HC, MacDonald WD (1999) Anisotropy of magnetic susceptibility in relation to source vents of ignimbrites: empirical observations. *Tectonophysics* 307:207–218 DOI 10.1016/S0040-1951(99)00126-2
- Palmer HC, MacDonald WD, Gromme CS, Elwood BB (1996) Magnetic properties and emplacement of the Bishop tuff, California. *Bull Volcanol* 58:101–116

- Pioli L (2003) High-grade ignimbrites from the Sulcis volcanic district (SW Sardinia, Italy): the example of Nuraxi tuff. PhD thesis. Università di Pisa, Pisa, Italy
- Pioli L, Rosi M (2005) Rheomorphic structures in a high-grade ignimbrite: The Nuraxi tuff, Sulcis volcanic district (SW Sardinia, Italy). *J Volcanol Geotherm Res* 142:11–28 DOI [10.1016/j.volgeores.2004.10.011](https://doi.org/10.1016/j.volgeores.2004.10.011)
- Potter DK, Stephenson A (1988) Single-domain particles in rocks and magnetic fabric analysis. *Geophys Res Lett* 15:1097–1100
- Quane SL, Russell JK (2005) Welding: insights from high-temperature analogue experiments. *J Volcanol Geotherm Res* 142:67–87 DOI [10.1016/j.volgeores.2004.10.014](https://doi.org/10.1016/j.volgeores.2004.10.014)
- Rochette P, Jackson M, Auburg C (1992) Rock magnetism and the interpretation of anisotropy of magnetic susceptibility. *Rev Geophys* 30:209–226
- Russell JK, Quane SL (2005) Rheology of welding: inversion of field constraints. *J Volcanol Geoth Res* 142:173–191 DOI [10.1016/j.volgeores.2004.10.017](https://doi.org/10.1016/j.volgeores.2004.10.017)
- Schlinger CM, Rosenbaum JG, Veblen DR (1988) Fe-oxide microcrystals in welded tuff from southern Nevada: origin of remanence carriers by precipitation in volcanic glass. *Geology* 16:556–559
- Sheridan MF, Ragan DM (1976) Compaction of ash-flow tuffs. In: Chilingar GV, Wolf KH (ed) *Compaction of coarse-grained sediments*, II. Elsevier, Amsterdam, pp 617–677
- Speranza F, Villa IM, Sagnotti L, Florindo F, Cosentino D, Cipollari P, Mattei M (2002) Age of the Corsica-Sardinia rotation and Liguro-provençal basin spreading: new paleomagnetic and Ar/Ar evidence. *Tectonophysics* 347:231–251 DOI [10.1016/S0040-1951\(02\)00031-8](https://doi.org/10.1016/S0040-1951(02)00031-8)
- Stephenson A (1994) Distribution anisotropy: two simple models for magnetic lineation and foliation. *Phys Earth Planet Int* 82:49–53
- Stephenson A, Sadikun S, Potter DK (1986) A theoretical and experimental comparison of the anisotropies of magnetic susceptibility and remanence in rocks and minerals. *Geophys J R Astr Soc* 84:185–200
- Tarling DH, Hrouda F (1993) *The magnetic anisotropy of rocks*. Chapman & Hall, London, pp 232
- Thomas IM, Moyer TC, Wikswo JP (1992) High resolution magnetic susceptibility imaging of geological thin sections: pilot study of a pyroclastic sample from the Bishop tuff, California, USA. *Geophys Res Lett* 19:2139–2142
- Van der Molen I, Paterson MS (1979) Experimental deformation of partially-melted granite. *Contrib Mineral Petrol* 70:299–318
- Vernon H (1987) A microstructural indicator of shear sense in volcanic rocks and its relationship to porphyroblast rotation in metamorphic rocks. *J Geology* 95:127–133
- Vigliotti L, Langenheim VE (1995) When did Sardinia stop rotating. New palaeomagnetic results. *Terra Nova* 7:424–435 DOI [10.1111/j.1365-3121.1995.tb00538.x](https://doi.org/10.1111/j.1365-3121.1995.tb00538.x)
- Wolff JA, Elwood BB, Sachs SD (1989) Anisotropy of magnetic susceptibility in welded tuffs: application to a welded-tuff dyke in the Tertiary Trans-Pecos Texas volcanic province, USA. *Bull Volcanol* 51:299–310
- Uyeda S, Fuller MD, Belsh JC, Girdler RW (1963) Anisotropy of magnetic susceptibility of rocks and minerals. *J Geophys Res* 68:279–291